MICROSTRUCTURAL ASPECTS OF INTERCONNECT FAILURE

J. SANCHEZ, E. ARZT
Max-Planck Institut für Metallforschung, and Institut für Metallkunde
University of Stuttgart, 92 Seestrasse, 7000 Stuttgart, Germany

ABSTRACT

The range of microstructural effects on thin film and interconnect properties is briefly described, and the improvement of interconnect reliability with increased strength is reviewed. We show that the strengthening effect of dispersed second phases depends on their resistance to coarsening during thermal treatments. The rapid coarsening of Θ phases during annealing and accelerated electromigration testing is reviewed, leading to a discussion of metallurgical factors which determine the coarsening behavior. We describe alloy systems expected to have reduced coarsening rates. We suggest that the recently reported increased reliability of Al-Sc interconnects is due to finely dispersed coherent phases which are particularly resistant to coarsening. The range of electromigration failure morphologies is illustrated with particular emphasis on transgranular slit failures. The failures are discussed in terms of diffusion pathways and models for failure.

INTRODUCTION

The reliability of Al alloy interconnects in integrated circuit (IC) devices is of paramount interest for IC manufacturers and users. Interconnect failures are due to electromigration and stress induced voiding processes. The processes which limit reliability are determined by the interconnect microstructure, which in turn may be influenced by the interconnect width and thickness. Interconnect microstructure includes grain size, grain size distribution, and grain crystallographic texture as well as the effects of alloying additions to the Al film. However the interconnect microstructure may evolve during annealing, reliability testing and device service, and the potential effect of microstructure changes on the interconnect performance may be profound. We shall briefly review the range of microstructural effects on film properties and interconnect lifetime.

Since metallizations are typically Al alloyed with Cu [1], Ti [2], Pd [3] and Sc [4], we shall include those microstructural aspects associated with alloying such as solute distributions and the distributions of dispersed second phases. We focus on potential effects of dispersed second phases on film and interconnect properties, and show that the potential beneficial effects of dispersed second phases, such as film strengthening, may depend on the relative stability of dispersed phases. Here we define "particle stability" as the resistance to coarsening during treatments such as annealing and accelerated electromigration testing. Using Al-Cu thin films and interconnects as an illustrative system for microstructural evolution we review the coarsening [5] of Al_2Cu Θ phases during annealing and the enhancement of Θ coarsening [6] during electromigration testing. Examples of electromigration failures located along coarsened Θ phases will be shown [6-8], which suggest a correlation between Θ coarsening and processes which limit interconnect lifetime. This leads to the proposal that increased interconnect reliability may depend in part upon improved particle stability. We review the metallurgical factors which determine the rate of particle coarsening, and illustrate that alloy systems such as Al-Pd, Al-Ti and Al-Sc alloys may provide more stable second phases and stronger films and interconnects. In particular the coherent Al_3Sc phases produced in the Al-Sc system are especially resistant to coarsening. We note that interconnects fabricated from these alloys have been shown to provide electromigration resistance comparable to or greater than the widely used Al-Cu alloys.

Finally, we illustrate the range [7] of morphology of electromigration damage and failures in Al and Al-Cu interconnects, including hillocks, whiskers, large equiaxed voids and transgranular slit failures. The morphology of these features will be discussed in terms of mechanisms for failure.

EFFECTS OF MICROSTRUCTURE-STRENGTH CORRELATIONS FOR FILMS AND INTERCONNECTS

Grain size (d) is the most obvious microstructural feature to affect interconnect reliability. Since electromigration diffusion processes occur primarily via boundary diffusion, increased grain size reduces the amount of diffusive flux along interconnects. This generally leads to an increase in the electromigration lifetime. Interconnect line width (W) also determines the grain structure. When

Mat. Res. Soc. Symp. Proc. Vol. 265. ©1992 Materials Research Society

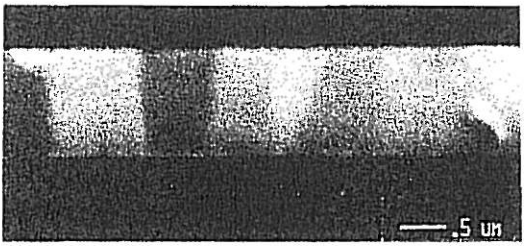

Fig. 1. Plan view focussed ion beam (FIB) micrograph of a bamboo grained Al-2% Cu interconnect 1.3 μm wide and 0.5 μm thick, showing contrast between different grains.

W/d ≈ 1, large segments of the interconnect are composed of bamboo grains as illustrated in figure 1 for a 1.3 μm wide Al-2% Cu interconnect. Obviously no boundary transport is possible in these line segments, and interconnects with W/d ≈1 and below show a significant increase in electromigration lifetime [9,10]. However the microstructure of narrow interconnects is not expected to be entirely bamboo [11]. Often electromigration damage occurs at those line segments containing a boundary path along the interconnect length, figure 2, which shows correlated void and hillock damage in a 1.8 μm wide Al interconnect. The effect of W/d on failure times has been modelled recently on the basis of grain boundary statistics in a line [20].

Film strength is also determined in part by grain size in an effect analogous to the "Hall-Petch" effect in bulk Al. Recent work [12] has shown that the yield strength (σ_f) of Al and Al-Cu films is the sum of film thickness (h) dependent and grain size dependent components, σ_h and σ_d, respectively,

$$\sigma_f = \sigma_h + \sigma_d = m/h + k/d^n \qquad (1),$$

where the coefficients (m) and (k) and the exponent (n ≈ 1/2) have been measured experimentally [12]. However it is not obvious that grain size strengthening occurs in unpassivated bamboo interconnects. Recent work [13] has demonstrated that the stress levels (or yield stresses) in narrow unpassivated Al-0.5% Cu interconnects were substantially below those in continuous films of the same alloy. The interconnects sustained relatively small uniaxial stresses (less than ≈ 80 MPa at temperatures above 200°C) aligned along the interconnect length, and were virtually stress free across the line width. Continuous films typically have uniform biaxial stresses and can sustain stresses of several hundred MPa. We conclude that grain size strengthening in continuous films does not directly translate to the strengthening of narrow interconnects. The possibility exists however that grain size may have some effect on the strength of passivated interconnects, since boundaries may play a role in stress relaxation processes which are limited by the passivation.

Interconnect crystallographic texture also helps to determine electromigration reliability. It has been shown that interconnects patterned from films with more uniform (111) texture have improved reliability [9,14,15]. It has been proposed that this effect is due to the tilt boundaries

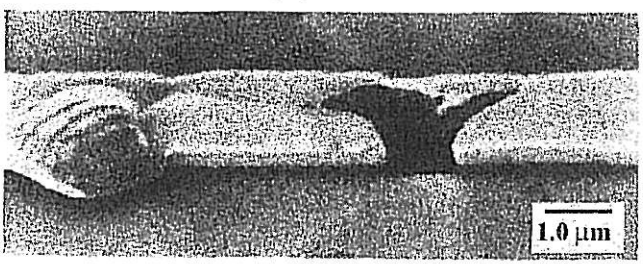

Fig. 2 FIB micrograph of electromigration damage in a laser reflowed Al interconnect 1.8 μm wide and 0.5 μm thick. Void and hillock are connected by a boundary parallel to line. (Electron flux was from right to left.)

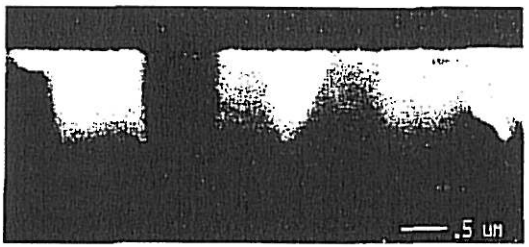

Fig. 1. Plan view focussed ion beam (FIB) micrograph of a bamboo grained Al-2% Cu interconnect 1.3 μm wide and 0.5 μm thick, showing contrast between different grains.

W/d = 1, large segments of the interconnect are composed of bamboo grains as illustrated in figure 1 for a 1.3 μm wide Al-2% Cu interconnect. Obviously no boundary transport is possible in these line segments, and interconnects with W/d ≈1 and below show a significant increase in electromigration lifetime [9,10]. However the microstructure of narrow interconnects is not expected to be entirely bamboo [11]. Often electromigration damage occurs at those line segments containing a boundary path along the interconnect length, figure 2, which shows correlated void and hillock damage in a 1.8 μm wide Al interconnect. The effect of W/d on failure times has been modelled recently on the basis of grain boundary statistics in a line [20].

Film strength is also determined in part by grain size in an effect analogous to the "Hall-Petch" effect in bulk Al. Recent work [12] has shown that the yield strength (σ_f) of Al and Al-Cu films is the sum of film thickness (h) dependent and grain size dependent components, σ_h and σ_d, respectively,

$$\sigma_f = \sigma_h + \sigma_d = m/h + k/d^n \qquad (1),$$

where the coefficients (m) and (k) and the exponent (n = 1/2) have been measured experimentally [12]. However it is not obvious that grain size strengthening occurs in unpassivated bamboo interconnects. Recent work [13] has demonstrated that the stress levels (or yield stresses) in narrow unpassivated Al-0.5% Cu interconnects were substantially below those in continuous films of the same alloy. The interconnects sustained relatively small uniaxial stresses (less than ≈ 80 MPa at temperatures above 200°C) aligned along the interconnect length, and were virtually stress free across the line width. Continuous films typically have uniform biaxial stresses and can sustain stresses of several hundred MPa. We conclude that grain size strengthening in continuous films does not directly translate to the strengthening of narrow interconnects. The possibility exists however that grain size may have some effect on the strength of passivated interconnects, since boundaries may play a role in stress relaxation processes which are limited by the passivation.

Interconnect crystallographic texture also helps to determine electromigration reliability. It has been shown that interconnects patterned from films with more uniform {111} texture have improved reliability [9,14,15]. It has been proposed that this effect is due to the tilt boundaries

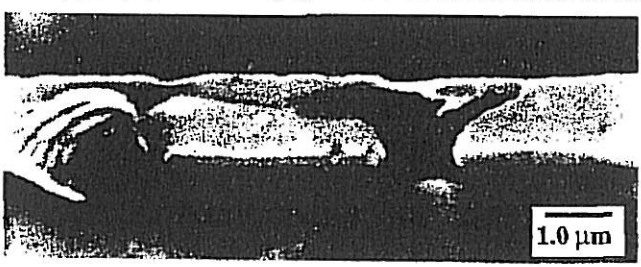

Fig. 2 FIB micrograph of electromigration damage in a laser reflowed Al interconnect 1.8 μm wide and 0.5 μm thick. Void and hillock are connected by a boundary parallel to line. (Electron flux was from right to left.)

formed between the {111} fiber oriented grains, where the boundary tilt axis is normal to the film plane. These boundaries [15] are expected to have a more uniform distribution in specific boundary energies and a (presumed) more uniform distribution in boundary diffusivities (D_{gb}). This microstructure will lead to a decrease in mass flux divergences at, for example, triple points. Randomly oriented grains will in general produce random boundaries with an increased distribution in D_{gb}, which is more likely to produce larger flux divergences and earlier failures.

Texture may also determine in part the strength levels in continuous films. The effect of crystal orientation on dislocation motion in films is shown in figure 3 [16]. We consider single phase films, capped with a surface (oxide) layer, on a rigid substrate. Dislocation glide is impeded by the top and bottom interfaces and by grain boundaries, as shown schematically in figure 3. The flow stress (σ_f) required for dislocations to glide on the plane indicated there is dependent on the film thickness as described by

$$\sigma_h = \frac{\sin\phi}{\cos\phi\ \cos\lambda}\ \frac{G^*\,b}{h} = C_{ijk}\frac{G^*\,b}{h} \qquad (2).$$

Here ϕ and λ are the included angles between the glide plane normal direction and Burgers vector and the film normal direction, respectively, and b is the Burgers vector. The constant C_{ijk} is defined for simplicity as = $\sin\phi / \cos\phi \cos\lambda$. The dislocation motion leaves trailing dislocation segments at the top and bottom of the film at the oxide/film and film/substrate interfaces, respectively, which leads to an effective shear modulus G* which is a detailed function [16] of the thicknesses and shear moduli of the film, oxide cap and substrate. The film thickness determines the width of the glide plane (L_h) for a given grain orientation by the factor $L_h = h / \sin\phi$, and the grain orientation also results in the resolved stress on the glide planes that is reduced from the applied stress by a factor ($\cos\phi \cos\lambda$). C_{ijk} thus helps determine the dependence of the film flow stress on grain orientation (ijk). We note that C_{111} is ≈ 3.46, while the average of the four lowest values of C_{110} for the available {111} <110> slip systems in (110) oriented grains is ≈ 1.42 [17]. Films of principally {111} textured grains will be stronger than {110} textured films, given equivalent grain sizes and film thicknesses. It is not known at present how variations in the strength level of variously textured grains along an interconnect will affect reliability. However interconnect stresses and stress relaxation processes have been proposed to affect electromigration lifetimes. Therefore the role of texture in determining reliability may in part be through the texture influence on the interconnect mechanical properties.

Effect of Mechanical Strength on Interconnect Reliability

We briefly review the proposed interactions between interconnect strength and electromigration reliability. On the basis of the "critical length" effect during electromigration in interrupted stripes, Blech [18] proposed that the electromigration mass flux may produce tensile and compressive stresses at regions of mass depletion and accumulation, respectively. The resulting stress gradients would induce mass fluxes in a direction opposite to the electromigration fluxes and would reduce the flux divergences and damage caused by the applied current. Since the stresses that may be produced are limited by the interconnect "yield" strength, stronger interconnects would be more

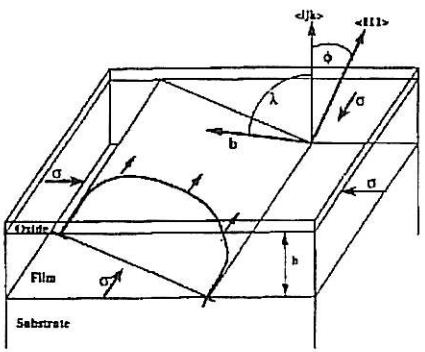

Fig. 3. Model for dislocation plasticity in thin films [16]. Here the dislocation bows between top and lower interfaces on glide plane (shaded). The film (grain) orientation helps to determine applied stress required for dislocation glide (see text).

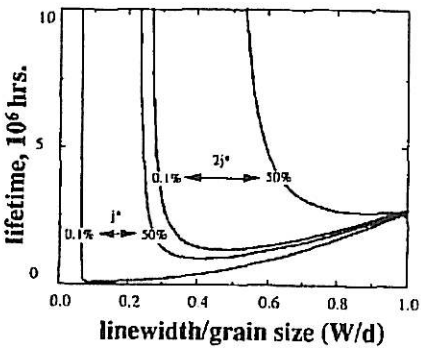

Fig. 4. Predicted effect of increased interconnect strength on the elecromigration lifetime for near bamboo interconnects as a function of linewidth/grain size ratio W/d. (After ref [20].)

resistant to electromigration damage since they would sustain larger stress gradients and induced back fluxes. This model has been extended to continuous lines under passivations [19]. In addition it has been shown [20] how an increase in strength of near bamboo interconnects may dramatically improve the electromigration reliability, figure 4. In this figure the critical current density j* is proportional to the interconnect strength, and it is shown that an increase in the strength (and j*) by a factor of two significantly increases the time for a 0.1% failure rate and for a 50% failure rate as the interconnect microstructure becomes more bamboo-like with decreasing ratio W/d.

Detailed understanding of the interactions between interconnect strength, large hydrostatic tensile stresses in passivated lines [21], stress relaxation processes and failure is lacking. However there is mounting evidence that mechanical strength should be a major consideration in the design of new metallization alloys. We may therefore describe possible methods for film and interconnect strengthening by the control of the microstructure and the proper choice of materials systems.

Mechanisms For Film and Interconnect Strengthening

Metallizations are typically alloyed with additions such as Cu, Ti, Pd and Sc in order to improve the interconnection reliability. However because of the limited solubility of these elements in Al, phases such as Al_2Cu, Al_3Ti, Al_4Pd and Al_3Sc are formed. Film and interconnect properties may be sensitive functions of the phase size and distribution. We shall briefly describe several probable effects of particles on film and interconnect strength.

Traditionally, strengthening in crystalline materials involves impeding dislocation motion by presenting barriers to glide such as dispersed second phases and grain boundaries. In the context of plasticity in films, figure 3, a potential effect of dispersed phases of mean radius (r) and volume fraction (f_v) is to block dislocation motion on the glide plane as shown on figure 5a. The mean distance between blocking obstacles (L_r), for the regime of low volume fraction of second phase, is given by $L_r \approx r\,(f_v/2)^{-1/2}$. Thus particle strengthening is expected when $L_r < L_h/2$, or when

$$\frac{r}{(f_v/2)^{1/2}} < \frac{h}{2\sin\phi} \qquad (3).$$

Choosing nominal values of $\phi = 45^\circ$ and $f_v = 0.05$, we calculate that dispersed particles of radius less than $r \approx 0.1$ μm are expected to strengthen a 1.0 μm film, while 0.5 μm thick films require particles of size $r \approx 0.05$ μm for strengthening by this mechanism.

An indirect mechanism of particle strengthening of films involves the particle pinning of boundary motion and the suppression of grain growth, leading to a retained small grain size. The grain size strengthening effect as described in equation 1 is illustrated in figure 5b. We note that such strengthening in Al films has also been observed in free standing films [22] and films deposited on Si substrates [23]. The effect of a dispersed phase of mean radius (r) and areal fraction (f_a) is to pin the grains at a size (d_p) given by [24]

$$d_p = (3.4\,r)\,f_a^{-1/2} \qquad (4).$$

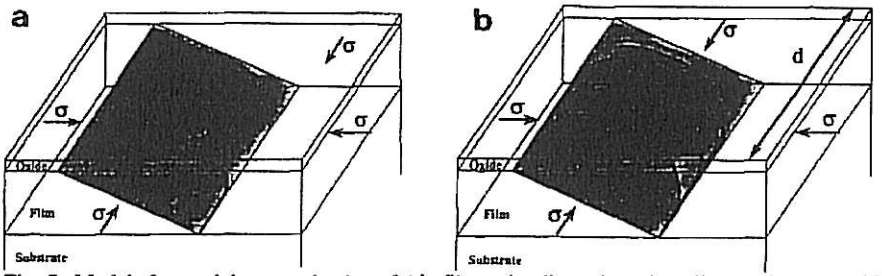

Fig. 5. Models for particle strengthening of thin films: a) a dispersion of small second phases will block dislocation motion, leading to strengthening; b) second phases (not shown) may maintain a small film grain size (d_p) leading to "Hall-Petch" type of strengthening.

The extent of this indirect strengthening may be calculated from the difference of the grain size dependent flow stress levels (σ_d) between single phase films (with grain size d) and films where particles have grains pinned at size d_p. Using equation 4 and $\sigma_d = k/d^n$ from equation 1 it can be shown that the fractional increase in film flow stress due to grain size pinning may be estimated as

$$(\sigma_{dp} - \sigma_d) / \sigma_d = (d / d_p)^{1/2} - 1 = (d\, f^{1/2} / 3.4\, r)^{1/2} - 1. \qquad (5).$$

We may estimate the magnitude of this effect for typical 1.0 μm thick films in which the annealed grain size is approximately twice [25,26] the film thickness, d ≈ 2.0 μm. Assuming that r ≈ 0.05 μm and $f_a \approx 0.05$, the fractional increase in film strength is significant, approximately $(\sigma_{dp} - \sigma_d) / \sigma_d \approx 0.62$. Again we note that the grain size strengthening effect in interconnects may not be operative to the same degree as in films. In fact reducing the interconnect grain size generally leads to reduced electromigration lifetimes. However the final effect of dispersed phases on reliability will be a combination of the strengthening and microstructural factors described above. A recent comparison [4] of the electromigration lifetimes of Al-Cu and Al-Sc alloys showed greater reliability of the Al-Sc interconnects in spite of a smaller grain size than in the Al-Cu interconnects.

We note that the beneficial effect of Cu additions on electromigration reliability is not due to a strengthening effect. Recent measurements found roughly equal strength levels in Al and Al-Cu films [12]. This is to be expected since the Θ phases found in the binary Al-Cu films reside along boundaries and triple points [27]. Considering the strengthening mechanisms described above, Θ phases with this morphology are expected to contribute little to the film or interconnect strength. The beneficial effect of copper additions in Al interconnects is generally agreed to be the reduction of grain boundary diffusivity due to Cu segregation to the boundaries.

θ COARSENING IN Al-2% Cu THIN FILMS AND INTERCONNECTS

Both mechanisms described above show that the efficiency of particle strengthening, at constant volume fraction, is increased for smaller mean particle radius. Thus a fine dispersion of particles *which remain small* during the thermal treatments of device fabrication is desirable. Particle size stability is determined by the rate of coarsening of the second phases. As an example, we review the kinetics of Θ particle size evolution during Ostwald coarsening in Al-2% Cu thin films during annealing. The enhancement of Θ coarsening during electromigration testing will also be presented. We then review those metallurgical factors which determine the coarsening rates of second phases and describe the characteristics of alloy systems which are expected to have improved particle stability and interconnect reliability. This leads to the suggestion that increased particle thermal stability, due to reduced second phase coarsening rates, may be a significant factor in the design of more reliable interconnect alloys.

Experimental

Al-2% (wt.) Cu thin films 0.5 μm thick were sputter deposited onto thermally oxidized (100) 100 mm Si substrates at a rate of 120 nm/minute without applied heating or substrate bias. Base

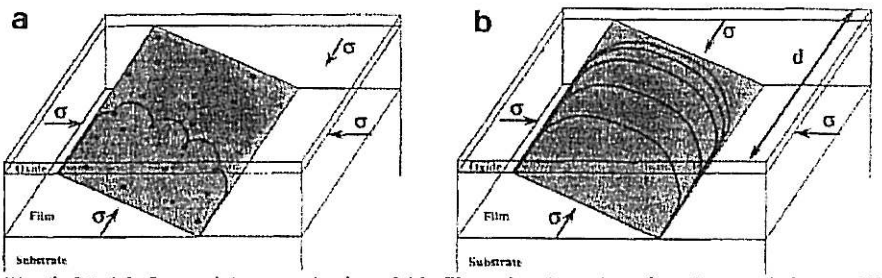

Fig. 5. Models for particle strengthening of thin films: a) a dispersion of small second phases will block dislocation motion, leading to strengthening; b) second phases (not shown) may maintain a small film grain size (d_p) leading to "Hall-Petch" type of strengthening.

The extent of this indirect strengthening may be calculated from the difference of the grain size dependent flow stress levels (σ_d) between single phase films (with grain size d) and films where particles have grains pinned at size d_p. Using equation 4 and $\sigma_d = k/d^n$ from equation 1 it can be shown that the fractional increase in film flow stress due to grain size pinning may be estimated as

$$(\sigma_{dp} - \sigma_d) / \sigma_d = (d / d_p)^{1/2} - 1 = (d f^{1/2} / 3.4\, r)^{1/2} - 1. \qquad (5).$$

We may estimate the magnitude of this effect for typical 1.0 μm thick films in which the annealed grain size is approximately twice [25,26] the film thickness, d ≈ 2.0 μm. Assuming that r ≈ 0.05 μm and $f_n \approx 0.05$, the fractional increase in film strength is significant, approximately $(\sigma_{dp} - \sigma_d) / \sigma_d \approx 0.62$. Again we note that the grain size strengthening effect in interconnects may not be operative to the same degree as in films. In fact reducing the interconnect grain size generally leads to reduced electromigration lifetimes. However the final effect of dispersed phases on reliability will be a combination of the strengthening and microstructural factors described above. A recent comparison [4] of the electromigration lifetimes of Al-Cu and Al-Sc alloys showed greater reliability of the Al-Sc interconnects in spite of a smaller grain size than in the Al-Cu interconnects.

We note that the beneficial effect of Cu additions on electromigration reliability is not due to a strengthening effect. Recent measurements found roughly equal strength levels in Al and Al-Cu films [12]. This is to be expected since the Θ phases found in the binary Al-Cu films reside along boundaries and triple points [27]. Considering the strengthening mechanisms described above, Θ phases with this morphology are expected to contribute little to the film or interconnect strength. The beneficial effect of copper additions in Al interconnects is generally agreed to be the reduction of grain boundary diffusivity due to Cu segregation to the boundaries.

θ COARSENING IN Al-2% Cu THIN FILMS AND INTERCONNECTS

Both mechanisms described above show that the efficiency of particle strengthening, at constant volume fraction, is increased for smaller mean particle radius. Thus a fine dispersion of particles *which remain small* during the thermal treatments of device fabrication is desirable. Particle size stability is determined by the rate of coarsening of the second phases. As an example, we review the kinetics of Θ particle size evolution during Ostwald coarsening in Al-2% Cu thin films during annealing. The enhancement of Θ coarsening during electromigration testing will also be presented. We then review those metallurgical factors which determine the coarsening rates of second phases and describe the characteristics of alloy systems which are expected to have improved particle stability and interconnect reliability. This leads to the suggestion that increased particle thermal stability, due to reduced second phase coarsening rates, may be a significant factor in the design of more reliable interconnect alloys.

Experimental

Al-2% (wt.) Cu thin films 0.5 μm thick were sputter deposited onto thermally oxidized (100) 100 mm Si substrates at a rate of 120 nm/minute without applied heating or substrate bias. Base

pressure of the sputter system was less than 2.0 10^{-5} mTorr. One wafer was sectioned into small (1 cm x 1 cm) sections which were annealed in forming gas in a hot wall tube furnace at 310°C for up to 40 minutes. Samples for transmission electron microscopy (TEM) were prepared with additional care taken to prevent inadvertant heating of the films. Measurements of Θ phase and Al grain size were obtained from TEM prints taken from several areas for each film condition. (See ref. [5] for details of sample preparation and phase size measurement.) In addition the films were examined in a scanning electron microscope (SEM) with an energy dispersive x-ray analysis (EDS) system. This allowed for the elemental characterization of local areas of interest in the film.

Other similar films were photolithographically patterned and etched to produce electromigration test circuits consisting of arrays of 25 interconnects in parallel. Line widths were from 1.0 μm to 6.0 μm, and line length was 1.5 mm. Prior to testing samples were annealed in forming gas at 425°C for 30 minutes. Wafer level accelerated electromigration testing on individually diced chips was performed as part of a larger study [7,8] of interconnect microstructure and electromigration failure analysis. Testing conditions were 1.75 10^6 A/cm^2 to 2.5 10^6 A/cm^2 and 175°C to 265°C. In addition pure Al interconnects were fabricated and tested. Their preparation is described in detail elsewhere [28,29], however several Al films were laser reflowed prior to patterning. The laser reflow process serves to locally anneal the metallization in order to improve film step coverage over device topology and to enlarge the film grain size. The grooves corresponding to the junction of grain boundaries and the film surface were readily apparent after the laser reflow process.

The microstructure of tested and untested but otherwise identically treated interconnects was observed with SEM, TEM and focussed ion beam (FIB) techniques. (The TEM results have been presented elsewhere [7,8,30].) The FIB induced secondary electron and ion yields are dependent upon the orientation of the target crystal with respect to the beam direction [31] and produce bright/dark contrast between grains of different crystallographic orientation in the film.

Results: θ Coarsening in Continuous Films

The as deposited Θ particles, about 200 nm in diameter, are uniformly distributed along grain boundaries and grain interiors [27]. Cross section TEM results on identical films show a relatively even dispersion of Θ through the film thickness ([27] and no evidence of the metastable Θ′ phases. Plan view TEM results [5] show the initiation of Θ phase coarsening at triple points after annealing for 5 minutes at 310°C, figure 6a. Annealing for 40 minutes at 310°C shows extensive Al growth and much larger Θ phases due to coarsening at triple points, figure 6b. The Θ particles remaining in the largest grain interiors, as shown in several grains in figure 6b, have also increased in size to about 0.06 μm for this anneal. Identical films annealed at 345°C have shown that coarsening has completely removed Θ phases in grain interiors after only 15 minutes [27]. It is also possible to detect the coarsened Θ phases in the SEM, figure 7a. Here the enhanced secondary electron emission provides bright contrast of the Θ phase for the same film condition as in figure 6b. These

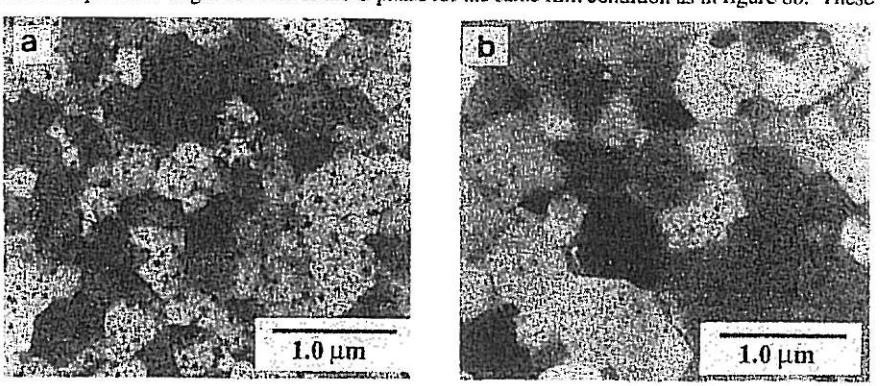

Fig. 6. Plan view TEM micrographs of 0.5 μm thick Al-2% Cu thin films after annealing for 5 minutes (a) and 40 minutes (b) at 310°C. Θ phases have black contrast and are shown to coarsen at triple points with continued annealing.

pressure of the sputter system was less than 2.0 10^{-5} mTorr. One wafer was sectioned into small (1 cm x 1 cm) sections which were annealed in forming gas in a hot wall tube furnace at 310°C for up to 40 minutes. Samples for transmission electron microscopy (TEM) were prepared with additional care taken to prevent inadvertant heating of the films. Measurements of Θ phase and Al grain size were obtained from TEM prints taken from several areas for each film condition. (See ref. [5] for details of sample preparation and phase size measurement.) In addition the films were examined in a scanning electron microscope (SEM) with an energy dispersive x-ray analysis (EDS) system. This allowed for the elemental characterization of local areas of interest in the film.

Other similar films were photolithographically patterned and etched to produce electromigration test circuits consisting of arrays of 25 interconnects in parallel. Line widths were from 1.0 μm to 6.0 μm, and line length was 1.5 mm. Prior to testing samples were annealed in forming gas at 425°C for 30 minutes. Wafer level accelerated electromigration testing on individually diced chips was performed as part of a larger study [7,8] of interconnect microstructure and electromigration failure analysis. Testing conditions were 1.75 10^6 A/cm^2 to 2.5 10^6 A/cm^2 and 175°C to 265°C. In addition pure Al interconnects were fabricated and tested. Their preparation is described in detail elsewhere [28,29], however several Al films were laser reflowed prior to patterning. The laser reflow process serves to locally anneal the metallization in order to improve film step coverage over device topology and to enlarge the film grain size. The grooves corresponding to the junction of grain boundaries and the film surface were readily apparent after the laser reflow process.

The microstructure of tested and untested but otherwise identically treated interconnects was observed with SEM, TEM and focussed ion beam (FIB) techniques. (The TEM results have been presented elsewhere [7,8,30].) The FIB induced secondary electron and ion yields are dependent upon the orientation of the target crystal with respect to the beam direction [31] and produce bright/dark contrast between grains of different crystallographic orientation in the film.

Results: Θ Coarsening in Continuous Films

The as deposited Θ particles, about 200 nm in diameter, are uniformly distributed along grain boundaries and grain interiors [27]. Cross section TEM results on identical films show a relatively even dispersion of Θ through the film thickness ([27] and no evidence of the metastable Θ′ phases. Plan view TEM results [5] show the initiation of Θ phase coarsening at triple points after annealing for 5 minutes at 310°C, figure 6a. Annealing for 40 minutes at 310°C shows extensive Al growth and much larger Θ phases due to coarsening at triple points, figure 6b. The Θ particles remaining in the largest grain interiors, as shown in several grains in figure 6b, have also increased in size to about 0.06 μm for this anneal. Identical films annealed at 345°C have shown that coarsening has completely removed Θ phases in grain interiors after only 15 minutes [27]. It is also possible to detect the coarsened Θ phases in the SEM, figure 7a. Here the enhanced secondary electron emission provides bright contrast of the Θ phase for the same film condition as in figure 6b. These

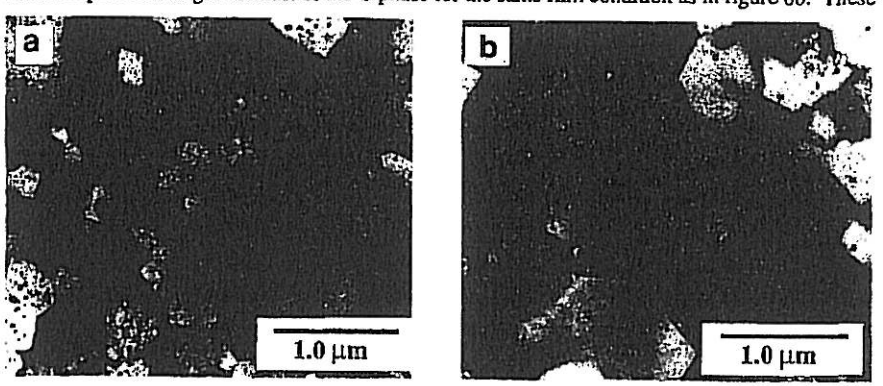

Fig. 6. Plan view TEM micrographs of 0.5 μm thick Al-2% Cu thin films after annealing for 5 minutes (a) and 40 minutes (b) at 310°C. Θ phases have black contrast and are shown to coarsen at triple points with continued annealing.

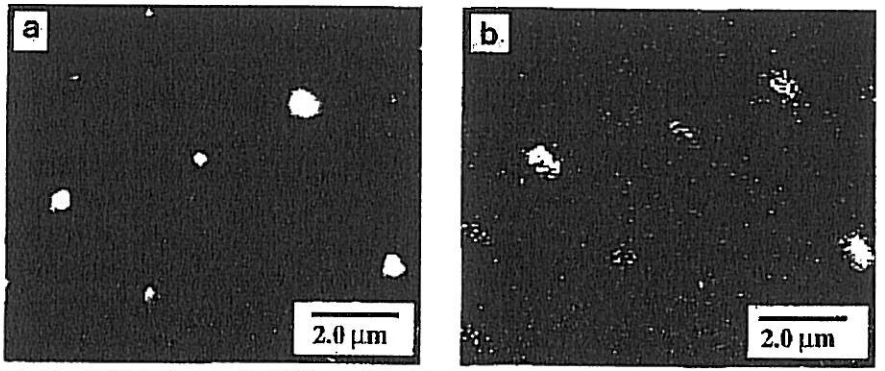

Fig. 7. a) SEM micrograph of 0.5 μm thick Al-2% Cu thin film after annealing for 40 minutes at 310°C (condition as in figure 6b). b) Energy analyzed x-rays from same area as in 7a showing enhanced Cu at bright areas, verifying these as Θ phases.

bright areas are further verified as the copper rich Θ phase by mapping of the copper x-rays generated by the incident electron beam and analyzed by the EDS. Figure 7b is an elemental copper mapping of the same area as in figure 7a, showing the correspondence between the bright areas in the secondary electron and copper x-ray mapping images. The bright contrast of Θ in the SEM will be useful for the subsequent correlation of electromigration damage with Θ phases after testing.

The coarsening rate of the triple point Θ is shown in figure 8. Note that the Θ size shows an initial period of rapid coarsening which decreases to steady state behavior after about 10 minutes. This initial period also corresponds to rapid initial grain growth of the aluminum, during which boundary migration may intersect additional small Θ phases previously in grain interiors, thereby increasing the Θ volume fraction and coarsening rate [5].

Enhanced θ Coarsening During Electromigration

Θ coarsening is enhanced [6] during accelerated electromigration testing as clearly shown in figure 9 for a 5.0 μm wide Al-2% Cu interconnect. The testing conditions were 250°C and 1.75 10^6 A/cm^2. The median time to failure (MTF) for this array was approximately 24 hours, however the circuit remained on the hot chuck for approximately 40 hours to allow for the failure of all of the interconnects in the circuit. SEM figure 9a shows the Θ phase size and distribution in an untested interconnect after completion of the test (i.e., 40 hrs. at 250°C). Figure 9b shows the Θ phase morphology in a tested interconnect adjacent to that in figure 9a. The enhancement of the coarsening process is evident since the effect of electromigration has been to increase the size and decrease the number of Θ phases, figure 9b. This effect is in contrast to a simple "Cu accumulation" effect [32] where the average concentration of Cu increases near the positive

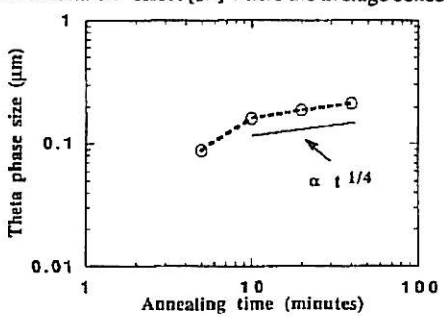

Fig. 8. Plot showing the increase of Θ phase size (radius) with annealing time at 310°C. After an initial period of rapid coarsening, a "steady state" coarsening rate proportional to $t^{1/4}$ is reached.

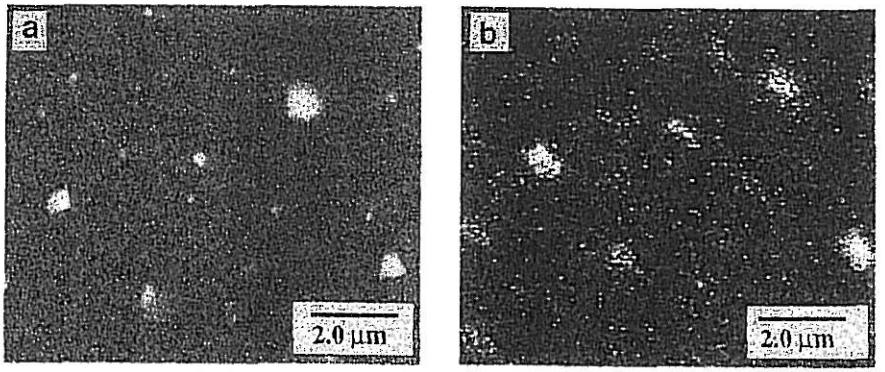

Fig. 7. a) SEM micrograph of 0.5 µm thick Al-2% Cu thin film after annealing for 40 minutes at 310°C (condition as in figure 6b). b) Energy analyzed x-rays from same area as in 7a showing enhanced Cu at bright areas, verifying these as Θ phases.

bright areas are further verified as the copper rich Θ phase by mapping of the copper x-rays generated by the incident electron beam and analyzed by the EDS. Figure 7b is an elemental copper mapping of the same area as in figure 7a, showing the correspondence between the bright areas in the secondary electron and copper x-ray mapping images. The bright contrast of Θ in the SEM will be useful for the subsequent correlation of electromigration damage with Θ phases after testing.

The coarsening rate of the triple point Θ is shown in figure 8. Note that the Θ size shows an initial period of rapid coarsening which decreases to steady state behavior after about 10 minutes. This initial period also corresponds to rapid initial grain growth of the aluminum, during which boundary migration may intersect additional small Θ phases previously in grain interiors, thereby increasing the Θ volume fraction and coarsening rate [5].

Enhanced θ Coarsening During Electromigration

Θ coarsening is enhanced [6] during accelerated electromigration testing as clearly shown in figure 9 for a 5.0 µm wide Al-2% Cu interconnect. The testing conditions were 250°C and 1.75 10^6 A/cm^2. The median time to failure (MTF) for this array was approximately 24 hours, however the circuit remained on the hot chuck for approximately 40 hours to allow for the failure of all of the interconnects in the circuit. SEM figure 9a shows the Θ phase size and distribution in an untested interconnect after completion of the test (i.e., 40 hrs. at 250°C). Figure 9b shows the Θ phase morphology in a tested interconnect adjacent to that in figure 9a. The enhancement of the coarsening process is evident since the effect of electromigration has been to increase the size and decrease the number of Θ phases, figure 9b. This effect is in contrast to a simple "Cu accumulation" effect [32] where the average concentration of Cu increases near the positive

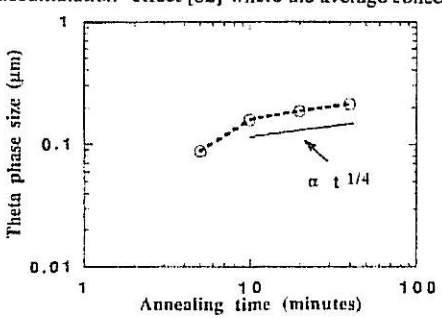

Fig. 8. Plot showing the increase of Θ phase size (radius) with annealing time at 310°C. After an initial period of rapid coarsening, a "steady state" coarsening rate proportional to $t^{1/4}$ is reached.

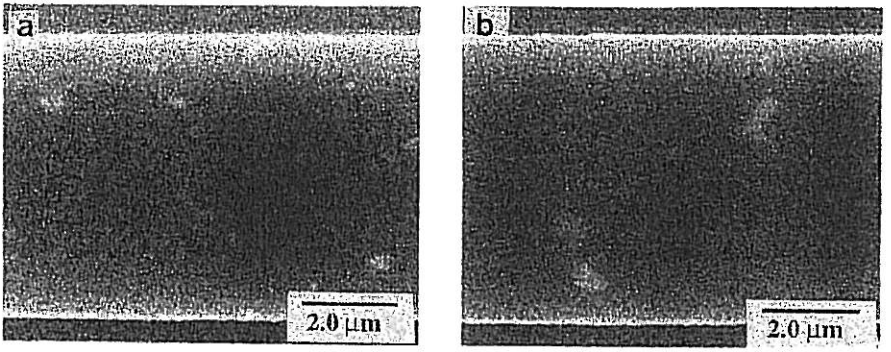

Fig. 9. Bright SEM contrast of Θ in an Al-2% Cu 5 µm wide interconnect after a) ≈ 40 hrs. at 250°C without current; b) identical interconnect and same thermal exposure as in figure 9a except with an applied current density of 1.75 10^6 A/cm^2, showing the enhancement of Θ phase coarsening during electromigration.

terminal of the line. Such a process would increase the size and/or the number of Θ phases in this region. However Cu accumulation at the positive end and depletion at the negative end of interconnects occurs by a process in which the coarsening mechanism is modified by the directional electromigration flux of Cu along the line. A detailed discussion of the effect of electromigration on the kinetics of coarsening is outside the scope of this discussion, however we note that electromigration will modify and increase the rate of coarsening.

The Θ coarsening enhancement is significant since often electromigration induced voiding occurs along such phases [7,8,30]. Figure 10 shows an example of a large erosion [7] void near Θ phases in an interconnect from the same array as shown in figure 9. Examination of 1.3 µm wide Al-2% Cu interconnects tested at the same conditions as above clearly show a failure, figure 11a, and mass accumulation and depletion damage, figure 11b, along coarsened Θ phases. The Θ shown in figure 11b have coarsened along bamboo boundaries, effectively serving as obstacles to mass flux. (The direction of electron and mass flux is from right to left in the micrographs of tested interconnects shown here.) Such blocking Θ phases are formed only by enhanced coarsening during electromigration.

Morphology of Interconnect Failures

FIB and SEM microscopy were used to determine the morphology of failures in relation to local grain structures. The damage and failures associated with coarsened Θ phases have been shown. Of particular interest are the transgranular slit failures previously observed in Al-Cu-Si lines [7,30].

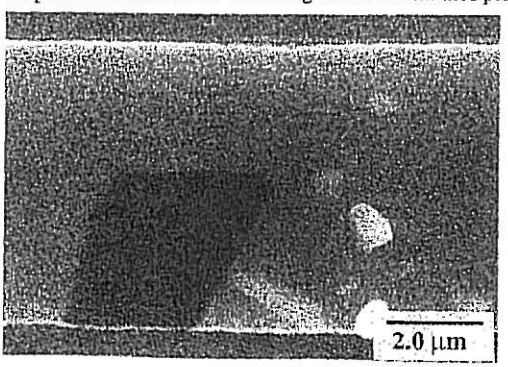

Fig. 10. SEM micrograph of electromigration tested Al-2% Cu 5.0 µm wide interconnect as in figure 9. Large erosion void is shown adjacent to coarsened Θ and hillocks. Current was from right to left.

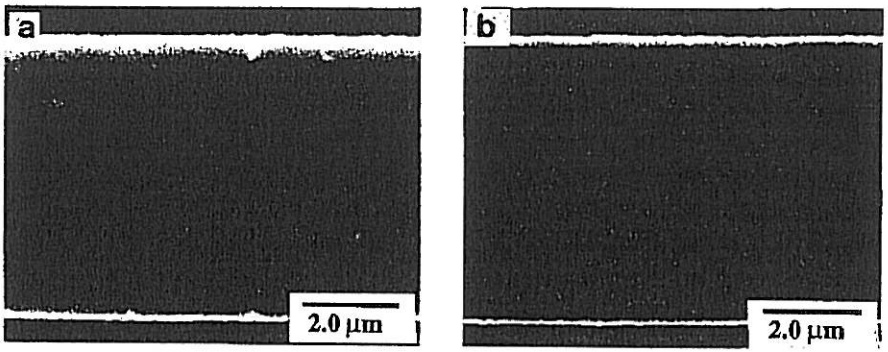

Fig. 9. Bright SEM contrast of Θ in an Al-2% Cu 5 μm wide interconnect after a) ≈ 40 hrs. at 250°C without current; b) identical interconnect and same thermal exposure as in figure 9a except with an applied current density of 1.75 10^6 A/cm^2, showing the enhancement of Θ phase coarsening during electromigration.

terminal of the line. Such a process would increase the size and/or the number of Θ phases in this region. However Cu accumulation at the positive end and depletion at the negative end of interconnects occurs by a process in which the coarsening mechanism is modified by the directional electromigration flux of Cu along the line. A detailed discussion of the effect of electromigration on the kinetics of coarsening is outside the scope of this discussion, however we note that electromigration will modify and increase the rate of coarsening.

The Θ coarsening enhancement is significant since often electromigration induced voiding occurs along such phases [7,8,30]. Figure 10 shows an example of a large erosion [7] void near Θ phases in an interconnect from the same array as shown in figure 9. Examination of 1.3 μm wide Al-2% Cu interconnects tested at the same conditions as above clearly show a failure, figure 11a, and mass accumulation and depletion damage, figure 11b, along coarsened Θ phases. The Θ shown in figure 11b have coarsened along bamboo boundaries, effectively serving as obstacles to mass flux. (The direction of electron and mass flux is from right to left in the micrographs of tested interconnects shown here.) Such blocking Θ phases are formed only by enhanced coarsening during electromigration.

Morphology of Interconnect Failures

FIB and SEM microscopy were used to determine the morphology of failures in relation to local grain structures. The damage and failures associated with coarsened Θ phases have been shown. Of particular interest are the transgranular slit failures previously observed in Al-Cu-Si lines [7,30].

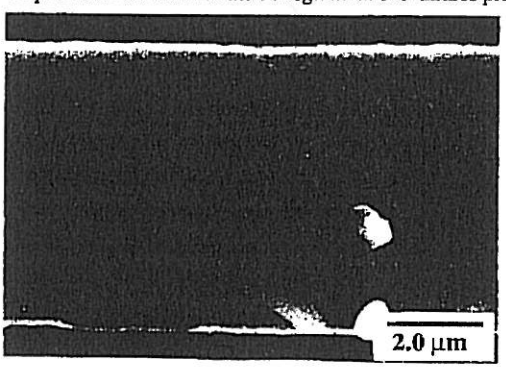

Fig. 10. SEM micrograph of electromigration tested Al-2% Cu 5.0 μm wide interconnect as in figure 9. Large erosion void is shown adjacent to coarsened Θ and hillocks. Current was from right to left.

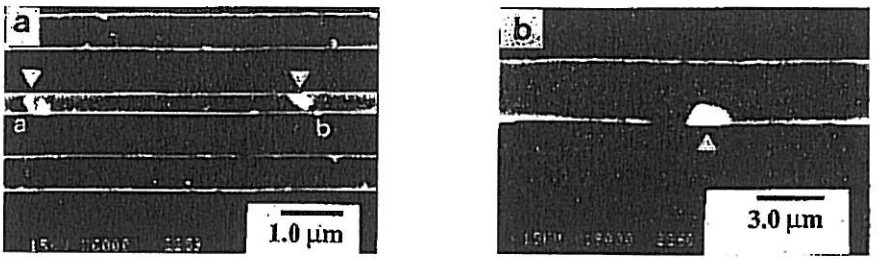

Fig. 11. Plan view SEM micrographs of electromigration damage at coarsened Θ (marked with arrows) in Al-2% Cu 1.3 µm wide interconnects. a) Shows voiding at region "a" and mass accumulation at "b". b) Shows a failure at the Θ phase (arrow). Current flux was right to left.

FIB figures 12a, b show a narrow failure in a laser reflowed Al interconnect in two orientations of tilt and rotation with respect to the ion beam. Each view provides different contrast in each grain, as described above. The relatively even contrast of material on either side of the void for both orientations suggests that the void is transgranular, but the evidence is not definitive. However the interesting change of contrast along the line indicated by the arrows does not correspond to a detectable surface groove. This may be explained as a low energy boundary or possibly a twin. A transgranular slit is clearly shown in figure 13a for a laser reflowed Al interconnect. The grain boundary is located along the line of contrast change, and the slit is shown by the arrows. Figure 13b is another view of the same slit, rotated 40° from the orientation in figure 13a to illustrate the even contrast across the slit. A final transgranular slit, figure 14, is shown to emanate from a small wedge void (at the black arrow), to traverse grain 2, and to cross the boundary between grains 2 and 3 while maintaining the same direction. The change in contrast between grains 1 and 2 indicates that the slit is *not* the site of the boundary that might have migrated into grain 2.

DISCUSSION

As shown in figure 8 the Θ coarsening kinetics at 310°C are described by the relation

$$r^4 - r_0^4 = Kt \qquad (5),$$

where r_0 is the initial phase radius, t is annealing time and K is a rate constant to be described below. This behavior is consistent with Ostwald coarsening controlled by solute diffusion along grain boundaries [33] and is described in more detail elsewhere [5].

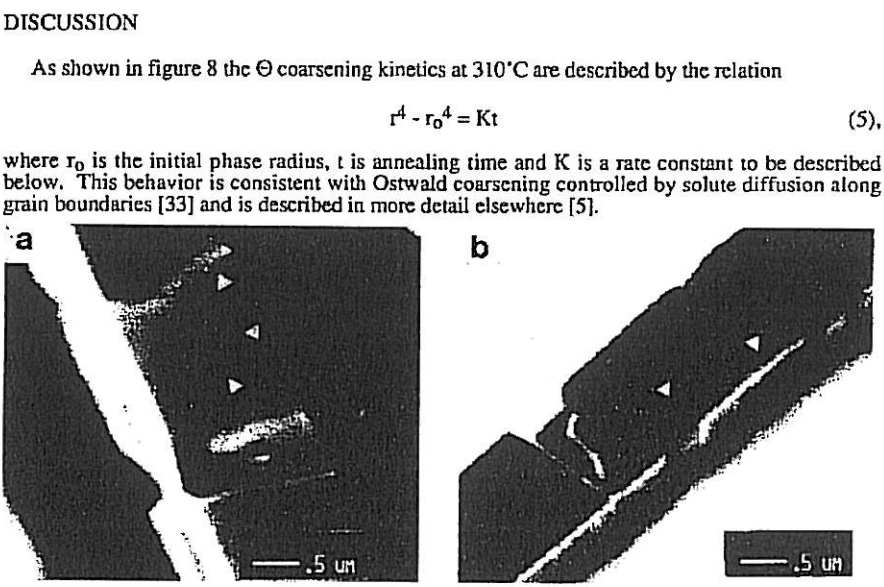

Fig. 12. FIB micrographs of slit failure in laser reflowed Al interconnects. a) Shows grain contrast, failure and a low angle or twin boundary (at arrows); sample tilted 45° normal to beam direction. b) Shows same sample tilted 35° from beam normal and rotated from position in 12a, showing change in grain contrast and the low angle or twin boundary (arrows).

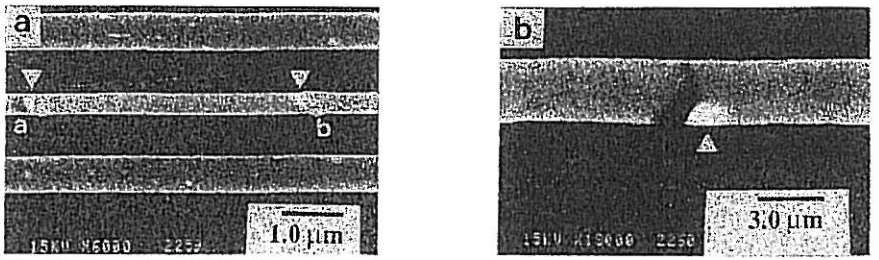

Fig. 11. Plan view SEM micrographs of electromigration damage at coarsened Θ (marked with arrows) in Al-2% Cu 1.3 µm wide interconnects. a) Shows voiding at region "a" and mass accumulation at "b". b) Shows a failure at the Θ phase (arrow). Current flux was right to left.

FIB figures 12a, b show a narrow failure in a laser reflowed Al interconnect in two orientations of tilt and rotation with respect to the ion beam. Each view provides different contrast in each grain, as described above. The relatively even contrast of material on either side of the void for both orientations suggests that the void is transgranular, but the evidence is not definitive. However the interesting change of contrast along the line indicated by the arrows does not correspond to a detectable surface groove. This may be explained as a low energy boundary or possibly a twin. A transgranular slit is clearly shown in figure 13a for a laser reflowed Al interconnect. The grain boundary is located along the line of contrast change, and the slit is shown by the arrows. Figure 13b is another view of the same slit, rotated 40° from the orientation in figure 13a to illustrate the even contrast across the slit. A final transgranular slit, figure 14, is shown to emanate from a small wedge void (at the black arrow), to traverse grain 2, and to cross the boundary between grains 2 and 3 while maintaining the same direction. The change in contrast between grains 1 and 2 indicates that the slit is *not* the site of the boundary that might have migrated into grain 2.

DISCUSSION

As shown in figure 8 the Θ coarsening kinetics at 310°C are described by the relation

$$r^4 - r_0^4 = Kt \qquad (5),$$

where r_0 is the initial phase radius, t is annealing time and K is a rate constant to be described below. This behavior is consistent with Ostwald coarsening controlled by solute diffusion along grain boundaries [33] and is described in more detail elsewhere [5].

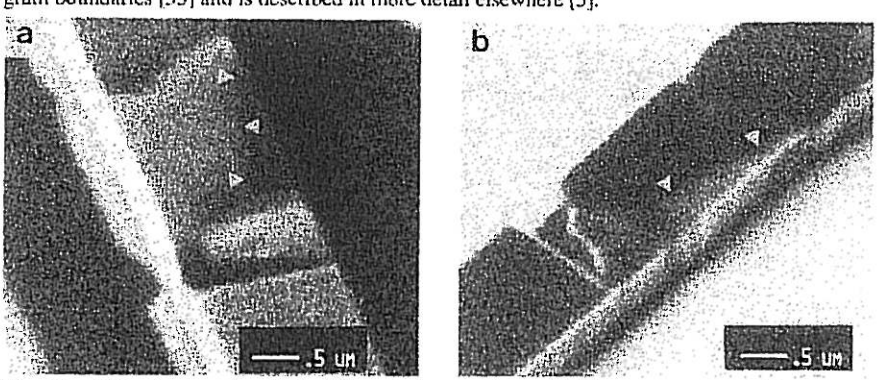

Fig. 12. FIB micrographs of slit failure in laser reflowed Al interconnects. a) Shows grain contrast, failure and a low angle or twin boundary (at arrows); sample tilted 45° normal to beam direction. b) Shows same sample tilted 35° from beam normal and rotated from position in 12a. showing change in grain contrast and the low angle or twin boundary (arrows).

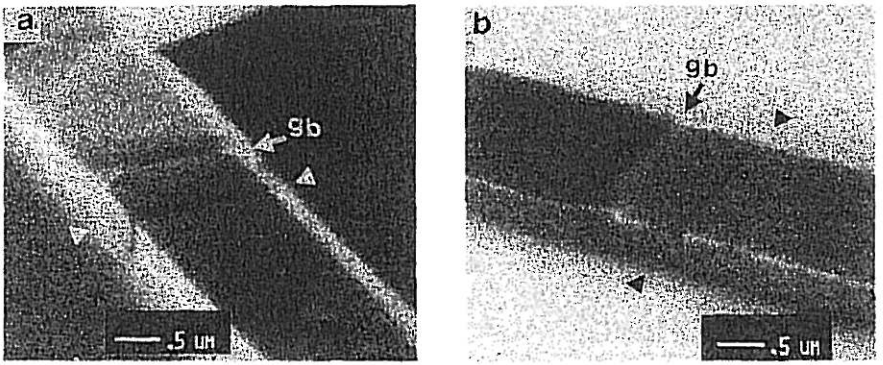

Fig. 13. FIB micrographs of transgranular slits in laser reflowed Al interconnects. a) Shows slit failure (at arrows) through the grain; sample tilted 45° from beam direction. b) Same sample tilted 55° from beam; even contrast across slit shows transgranular nature of slit.

K is given by [33]

$$K = \frac{4\,\gamma_i\,C_e\,D_{gb}\,\delta\,\Omega}{3\,A\,k\,T} \qquad (6),$$

where γ_i is the interphase (particle/matrix) boundary energy, C_e is the equilibrium solute concentration, D_{gb} is the solute boundary diffusivity, δ is the boundary thickness, Ω is the atomic volume, A is a geometrical constant, k is Boltzmann's constant and T is the absolute temperature. (In this discussion we neglect the effect of second phase stochiometry on the coarsening behavior.) If we assume that second phase stability is desirable for improved interconnect reliability, then optimal alloying additions to Al would be those in which γ_i, C_e and D_{gb} are reduced.

The interphase energy γ_i depends principally on the chemical and structural (i.e., crystal structure and crystallographic) differences between the matrix and second phase. However γ_i is reduced by at least an order of magnitude [34] by coherency between the two phases. C_e is obviously a minimum for insoluble alloying additions, while an a priori choice for a solute with decreased boundary diffusivity in Al is less obvious.

Al-Cu binary alloys typically form the incoherent Θ phase located at boundaries [27]. The rapid

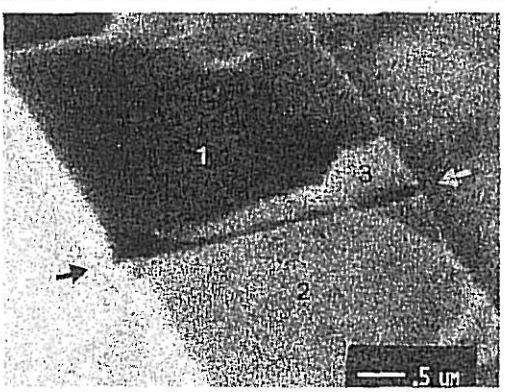

Fig. 14. FIB micrograph of transgranular slit failure (arrows) in Al interconnect, tested at 1.75 10^6 A/cm^2, showing the slit to traverse grain 2 and cross the boundary between grains 2 and 3.

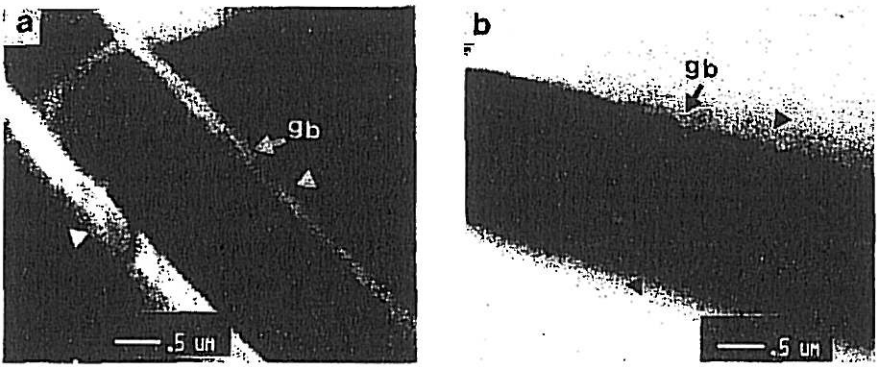

Fig. 13. FIB micrographs of transgranular slits in laser reflowed Al interconnects. a) Shows slit failure (at arrows) through the grain; sample tilted 45° from beam direction. b) Same sample tilted 55° from beam; even contrast across slit shows transgranular nature of slit.

K is given by [33]

$$K = \frac{4\,\gamma_i\,C_e\,D_{gb}\,\delta\,\Omega}{3\,A\,k\,T} \qquad (6),$$

where γ_i is the interphase (particle/matrix) boundary energy, C_e is the equilibrium solute concentration, D_{gb} is the solute boundary diffusivity, δ is the boundary thickness, Ω is the atomic volume, A is a geometrical constant, k is Boltzmann's constant and T is the absolute temperature. (In this discussion we neglect the effect of second phase stochiometry on the coarsening behavior.) If we assume that second phase stability is desirable for improved interconnect reliability, then optimal alloying additions to Al would be those in which γ_i, C_e and D_{gb} are reduced.

The interphase energy γ_i depends principally on the chemical and structural (i.e., crystal structure and crystallographic) differences between the matrix and second phase. However γ_i is reduced by at least an order of magnitude [34] by coherency between the two phases. C_e is obviously a minimum for insoluble alloying additions, while an a priori choice for a solute with decreased boundary diffusivity in Al is less obvious.

Al-Cu binary alloys typically form the incoherent Θ phase located at boundaries [27]. The rapid

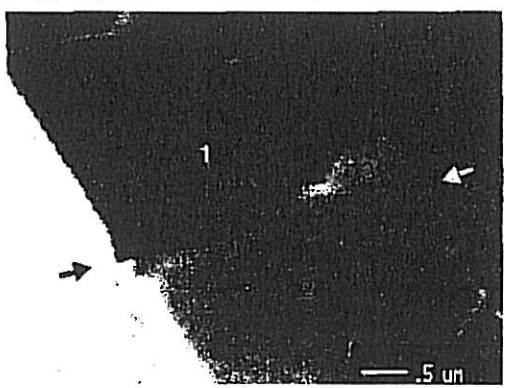

Fig. 14. FIB micrograph of transgranular slit failure (arrows) in Al interconnect, tested at 1.75 10^6 A/cm^2, showing the slit to traverse grain 2 and cross the boundary between grains 2 and 3.

coarsening of Θ shown above is due to the high γ_i between Θ and Al [35] and the rapid increase in C_e (Cu in Al) with temperature. Among the additions to Al proposed for improved reliability, Ti, Pd and Sc are virtually insoluble in Al. The boundary diffusivities of these solutes and the coarsening behavior of the Al_3Ti, Al_4Pd and Al_3Sc precipitate structures have not been characterized for thin films. We note however that all three systems have shown substantially improved electromigration resistance. The reliability of Al-0.15 wt.% Sc interconnects was recently shown [4] to be significantly improved over that of similarly treated Al-0.5 wt.% Cu lines. TEM microscopy of the Al-Sc films revealed strain field contrast characteristic of small coherent phases. Other recent work [36] has characterized the microstructure and the efficient strengthening effects of Al_3Sc phases in bulk Al-Sc alloys. There the Al_3Sc phases were shown (by lattice imaging TEM [36]) to be coherent, less than 0.01 μm in diameter and to similarly provide the strain field contrast at lower magnifications as observed in the thin film-interconnect study. Thus we propose that improved reliability of the Al-Sc alloy is dependent on the finely dispersed coherent Al_3Sc phases which retain their beneficial effect due to their resistance to coarsening. Further work is required in order to determine the effect of Ti, Pd and Sc additions on solute diffusivities, precipitate structures, film and interconnect properties and interconnect reliability.

Electromigration damage at coarsened Θ phases is inconsistent with models which require local Cu (and Θ) depletion prior to flux divergences. Voiding at Θ is more likely to limit lifetimes for interconnects with W/d ≈1, since blocking Θ phases and associated damage easily produce failures. Reducing the Θ (or Cu) volume fraction may minimize this failure mechanism, while a more fundamental approach is to choose an alloy resistant to coarsening as described above.

The transgranular slit morphology is intriguing since the generally accepted electromigration diffusion processes are limited to boundaries. However careful examination of the damage shows that often other pathways must operate. The blocking Θ phases along bamboo boundaries (see also [6,7,8]) are examples of alternative pathway mass transport. Further it is not obvious that the small volume slit void growth is controlled by diffusive processes. Local stresses or stress concentrations may induce plasticity which induces a "crack-like opening" to occur. The restraint of the substrate to the adhering interconnect prevents a simple "fracture" interpretation of slits. However the strengthening effect of small coherent phases may act to reduce the effects of stress induced voiding. The reliability increase of Al_3Sc interconnects was attributed in part to elimination of slit voiding [4]. It may be significant that transgranular slits appear to originate at wedge voids at the top edge-corner of the line, which may induce local stress concentrations. Similar wedge voids have been observed in passivated single crystal interconnects [37]. We note that slit voids (not always transgranular) are a common mode for stress induced failures.

TEM examination of a stress induced failure [37] showed that the parallel faces of the slit, which were vertical in the line, were both (111) type faces, consistent with a transgranular morphology. This orientation indicates that the material at the slit was not the typical (111) fiber texture but with an orientation of the type $(1\bar{1}0)$ or similarly normal to (111) planes. Work is in progress to determine possible relationships between interconnect texture and slit failures.

The range of failure morphologies generally observed for various interconnect materials under broad testing conditions suggests that a simple mechanistic analysis of failure time distributions is complicated at best. Hopefully future experimental work will focus on the determination of lifetimes of specific failure modes.

CONCLUSIONS

(1) Models for the effects of interconnect strength on reliability have been reviewed.

(2) Mechanisms for second phase strengthening of films and (possibly) interconnects have been outlined.

(3) Strengthening effects of dispersed phases have been shown to depend critically on their thermal stability, defined as the resistance to coarsening.

(4) The coarsening kinetics of Θ phases in Al-2% Cu thin films during annealing were shown to be proportional to $t^{1/4}$, consistent with Ostwald ripening controlled by grain boundary diffusion.

(5) Accelerated electromigration testing was shown to enhance Θ phase coarsening in Al-2% Cu interconnects.

(6) Electromigration induced damage and failures occurred adjacent to coarsened Θ phases, inconsistent with Cu depletion models for interconnect reliability.

(7) Transgranular slit failures were found in Al interconnects, inconsisistent with electromigration processes requiring grain boundary diffusion.

ACKNOWLEDGEMENTS

We acknowledge the assistance of L.T.McKnelly and S. Bader with sample preparation, O.Kraft and R. Young (FEI Company, Cambridge, UK) with SEM and FIB microscopy. One author (JES) would like to acknowledge the support of the Max-Planck Society during his tenure in Stuttgart, Germany.

REFERENCES

1. F. M. D'Heurle, Met. Trans., 2, 683 (1971).
2. F. Fischer, F. Neppl, in Proc. IEEE International Reliability Physics Symposium, (IEEE publishers, Las Vegas, 1984), vol. 1984, pp. 190-192.
3. Y. Koubuchi, J. Onuki, M. Suwa, S. Fukada, in Proc. VLSI Multilevel Interconnection Con. (IEEE publishers, Santa Clara, Ca., 1989), vol. TH-0259-2/89/0000-0419, pp. 419-425.
4. S.-I. Ogawa, H. Nishimura, in Proc. IEEE International Conference on Electron Devices and Materials (IEEE publishers, 1991), vol. IEEE-IEDM 1991, pp. 10.4.1-10.4.4.
5. J.E. Sanchez, Jr., L.T. McKnelly, J.W. Morris, Jr., in Phase Transformation Kinetics in Thin Films , edited by M. Chen (Mater. Res. Soc. Proc. 230, Pittsburgh, PA, 1991) pp. 67-72
6. J.E. Sanchez, Jr., O. Kraft, E. Arzt, in Proc. First International Workshop on Stress Induced Phenomena in Metallizations (American Institute of Physics, Ithaca, NY, 1991)
7. J.E. Sanchez, Jr., L.T. McKnelly, J.W. Morris Jr., J. Electron Mater., 19, 1213 (1990).
8. J.E. Sanchez, Jr., J.W. Morris Jr., in Materials Reliability Issues in Microelectronics, edited by J.R. Lloyd et al (Mater. Res. Soc. Proc. 225, Pittsburgh, PA, 1991) pp. 53-58
9. S. Vaidya, A.K. Sinha, Thin Solid Films, 75, 253 (1981).
10. J. Cho, C.V. Thompson, Appl. Phys. Lett., 54 , 2577 (1989).
11. D.T. Walton, H.J. Frost, C.V. Thompson, in Materials Reliability Issues in Microelectronics, edited by J.R. Lloyd et al (Mater. Res. Soc. Proc. 225, Pittsburgh, PA, 1991) pp. 219-224
12. R. Venkatraman, J.C. Bravman, to appear in J. Mater. Res. (1992).
13. P.R. Besser, R. Venkatraman, S. Brennan, J.C. Bravman, in Thin Film Stresses and Mechanical Properties III, edited by W.D. Nix et al (Mat. Res. Soc. Proc. 239, Pitts., PA, 1991)
14. M.J. Attardo, R. Rosenberg, J. Appl. Phys., 41, 2381 (1970).
15. D.B. Knorr, D. Tracy, K. P. Rodbell, Appl. Phys. Lett., 59, 3241 (1991).
16. W.D. Nix, Metallurgical Transactions A, 20A, 2217 (1989).
17. J.E. Sanchez Jr., E. Arzt, to appear in Scripta Metallurgica et Materialia, (1992).
18. I.A. Blech, C. Herring, Appl. Phys. Lett., 29, 131 (1976).
19. C.A. Ross, J.S. Drewery, R.E. Somekh, J.E. Evetts, J. Appl. Phys., 66, 2349 (1989).
20. E. Arzt, W.D. Nix, J. Mater. Res., 6, 731 (1991).
21. B. Greenebaum, A.I. Sauter, P.A. Flinn, W.D. Nix, Appl. Phys. Lett., 58, 1845 (1991).
22. A.J. Griffin, F.R. Brotzen, C. Dunn, Scripta Metallurgica, 20, 1271 (1986).
23. M. Doerner, D.S. Gardner, W.D. Nix, J. Mater. Res., 1, 845 (1986).
24. D.J. Srolovitz, M.P. Anderson, G.S. Grest, P.S. Sahni, Acta Metallurgica, 32, 1429 (1984).
25. W.W. Mullins, Acta Metallurgica, 6, 414 (1958).
26. J.E. Sanchez, Jr., E. Arzt, Scripta Metallurgica et Materialia, 26, 1325-1330 (1992).
27. D.R. Frear, J.E. Sanchez, Jr., A.D. Romig, J.W. Morris, Met. Trans A, 21A, 2449 (1990).
28. E. Arzt, O. Kraft, J.E. Sanchez, Jr., S. Bader, W.D. Nix, in Thin Films: Stresses and Mechanical Properties III, edited by W.D. Nix (Mat. Res. Soc. Proc. 239, Boston, MA, 1991)
29. O. Kraft, J.E. Sanchez, Jr., E. Arzt, in Materials Reliability Issues in Microelectronics II, edited by J.R. Lloyd et al (Mater. Res. Soc. Proc. 265, Pittsburgh, PA, 1992)
30. J.E. Sanchez, Jr., L.T. McKnelly, J.W. Morris, Jr., submitted Appl. Phys. Lett., (1991).
31. P.H. La Marche, R. Levi-Setti, K. Lam, IEEE Trans. Nucl. Sci., NS-30, 1240 (1983).
32. A.J. Learn, J. Electron. Mater., 3, 531 (1974).
33. M V. Speight, Acta Metallurgica, 16, 133 (1968).
34. J.J. Hoyt, S. Spooner, Acta Metallurgica et Materialia, 39, 689 (1991).
35. H.B. Aaron, H.I. Aaronson, Acta Metallurgica, 18, 699 (1970).
36. R.R. Sawtell, Ph.D Thesis, University of California, Berkeley, Dept. of Mat. Sci., (1988).
37. M. Hasunuma, et al., in Proc. IEEE International Conference on Electron Devices and Materials (IEEE publishers, Washington, DC 1989), vol. IEEE-IEDM 1989, pp. 677-680.